Phase Diagram of Ternary Cholesterol/Palmitoylsphingomyelin/Palmitoyloleoyl-Phosphatidylcholine Mixtures: Spin-Label EPR Study of Lipid-Raft Formation

Irina V. Ionova, Vsevolod A. Livshits, and Derek Marsh*
Centre of Photochemistry, Russian Academy of Sciences, Moscow, Russia; and Max-Planck-Institut für biophysikalische Chemie, Göttingen, Germany

ABSTRACT   For canonical lipid raft mixtures of cholesterol (chol), N-palmitoylsphingomyelin (PSM), and 1-palmitoyl-2-oleoyl-phosphatidylcholine (POPC), electron paramagnetic resonance (EPR) of spin-labeled phospholipids—which is insensitive to domain size—is used to determine the ternary phase diagram at 23°C. No phase boundaries are found for binary POPC/chol mixtures, nor for ternary mixtures with PSM content <24 mol %. EPR lineshapes indicate that conversion from the liquid-disordered (L_α) to liquid-ordered (L_o) phase occurs continuously in this region. Two-component EPR spectra and several tie lines attributable to coexistence of gel (L_β) and fluid phases are found for ternary mixtures with low cholesterol or low POPC content. For PSM/POPC alone, coexistence of L_α and L_β phases occurs over the range 50−95.5 mol % PSM. A further tie line is found at 3 mol % chol with endpoints at 50 and ≥77 mol % PSM. For PSM/chol, L_β−L_o coexistence occurs over the range 10−38 mol % chol and further tie lines are found at 4.5 and 7 mol % POPC. Two-component EPR spectra indicative of fluid-fluid (L_α−L_o) phase separation are found for lipid compositions: 25%<PSM<65%, 5%<chol<30–35%, 65%>POPC>10%, and confirmed by nonlinear EPR. Tie lines are identified in the L_α−L_o coexistence region, indicating that the fluid domains are of sufficient size to obey the phase rule. The three-phase triangle is bounded approximately by the compositions 40 and 75 mol % PSM with 10 mol % chol, and 60 mol % PSM with 25 mol % chol. These studies define the compositions of raft-like L_o phases for a minimal realistic biological lipid mixture.

INTRODUCTION

There is now accumulating evidence that the in-plane organization of plasma membranes is heterogeneous and contains lateral nanodomains enriched in cholesterol and sphingolipids (lipid rafts) that supposedly function as platforms for self-assembly and transport of specific protein complexes involved in signal transduction, and in membrane traffic within the cell (1–3). To gain insight into the formation and properties of such domains it is useful to study well-defined bilayer membranes that have simplified lipid compositions similar to those of cell membranes. Mixtures of a lipid with high chain-melting temperature (of which sphingolipids are representative) and cholesterol are of central interest because these are known to form the so-called liquid-ordered phase, L_o (4,5). The latter is distinguished from the usual liquid-disordered (or L_α) phase by having high local orientational order, but still retaining the long-range translational disorder that is characteristic of fluid lipid membranes.

A recent critical survey of phospholipid/cholesterol binary phase diagrams has revealed that direct experimental evidence for the existence of L_o-phases is, however, not so extensive as is generally assumed (6). This is especially the case for coexistence with the fluid L_α-phase, which is presumed to correspond with the formation of lipid rafts in biological membranes. It has long been recognized that coexistence of immiscible fluid phases (as opposed to gel-fluid coexistence) is most likely to be of biological significance (7). Direct evidence for coexistence of fluid L_α- and L_o-phase domains is somewhat more abundant in ternary systems, as found in a compendium of phase diagrams for mixtures of a high-melting lipid and a low-melting lipid with cholesterol (8). The lipid with low chain-melting temperature in these ternary mixtures is representative of the glycerophospholipid components of biological membranes, which mostly have an unsaturated chain at the sn-2 position.

There is, nevertheless, not entire agreement in the literature between the various phase diagrams for ternary mixtures that display fluid-fluid phase separation, nor in their interpretation (see (9,8)). This can be traced in part to the different techniques employed for visualizing domains or detecting phase separation. Optical microscopy requires the domains to be large, $\approx 300−500$ nm in diameter (10–13), as does ^{2}H-NMR spectroscopy of fluid phases, diameter $\gg 30−50$ nm at the very least (14–16). On the other hand, spin-label electron paramagnetic resonance (EPR) spectroscopy can resolve very small domains, diameter $\gg 1−2$ nm (17–20), and, for fluorescence resonance energy transfer (FRET), the minimum domain size is intermediate corresponding to $R_o \sim 2−8$ nm depending on the donor-acceptor pair (21,22). The relevance of small domains and limitation by R_o is found in FRET studies of a raft lipid mixture (23). Added to this, there is the complication that strong illumination in fluorescence microscopy

can induce photochemical reactions that artificially give rise to lipid domain formation (12,24). In view of all the above, it clearly is desirable to compare the results from different techniques to obtain a complete picture of domain formation.

Here, we concentrate on the canonical ternary lipid raft mixture, N-palmitoylsphingomyelin/1-palmitoyl-2-oleoyl phosphatidylcholine/cholesterol (PSM/POPC/chol), that was introduced originally by Prieto and colleagues (25,22). PSM is a representative high-melting raft sphingolipid, and POPC is a low-melting glycerolipid with the natural sn-2 chain unsaturation. Consequently, this ternary mixture is considered representative of the main lipid constituents in the outer leaflet of many mammalian cell plasma membranes (26).

A ternary phase diagram was first proposed for the PSM/POPC/chol system based on measurement of various spectroscopic parameters of lipid-soluble fluorophores: fluorescence anisotropy, averaged lifetime, and quenching by spin-labeled fatty acid (25). This diagram is characterized by a broad $L_\alpha-L_o$ phase coexistence region at low PSM/POPC ratios, a considerable region of $L_\beta-L_o$ phase coexistence at high PSM/POPC ratios, a $L_\alpha-L_\beta$ coexistence region at low cholesterol contents, and a three-phase triangle in the central part of the ternary diagram. In a subsequent study of the same system, coexisting fluid lipid domains were observed directly by fluorescence microscopy of giant vesicles (11). However, the phase diagram deduced from microscopy, although broadly the same, was essentially different in several significant details from that proposed in reference (25). In particular, fluid-fluid coexistence was observed only at higher mole fractions of PSM, and uniform membranes without domains were seen at high mole fractions of POPC.

So far, the phase diagram of PSM/POPC/chol mixtures has not been studied by spectroscopic techniques other than fluorescence, although there are two studies with brain sphingomyelin (bSM) from mammalian sources that employ other techniques (27,28). In the present work, spin-label EPR techniques are used to study the phase behavior and dynamics of the PSM/POPC/chol system. Conventional EPR is augmented by nonlinear EPR because the out-of-phase, first-harmonic, absorption spectra are able to separate overlapping EPR signals with differing spin-lattice relaxation times (29,30). Particular attention is paid to detecting possible $L_\alpha-L_o$ phase coexistence, especially at low PSM content where the published phase diagrams differ. Considerable effort is also invested in identifying tie lines, because these define the conversion between phases of fixed composition, and also the boundaries of the three-phase triangle, as well as the position of any critical points. Tie lines have been identified successfully by ^{2}H-NMR in phosphatidylcholine/phosphatidylcholine/cholesterol ternary mixtures (14–16), but until now not in sphingolipid-containing systems such as PSM/POPC/chol.

MATERIALS AND METHODS

Materials

POPC and PSM were from Avanti Polar Lipids (Alabaster, AL), and cholesterol (chol) from Sigma-Aldrich (Taufkirchen, Germany). Phosphatidylcholines spin-labeled in the sn-2 chain, 1-acyl-2-[n-(4,4-dimethyloxazolladine-N-oxyl)]stearoyl-sn-glycero-3-phosphocholine with $n = 14$ or 16 (14-PCSL and 16-PCSL), were synthesized as described (31).

Sample preparation

Total lipid mixture (2 μmol) and 0.5 mol % of spin label were codissolved in chloroform or chloroform/methanol (2:1 v/v) and evaporated under a stream of dry nitrogen gas. Residual solvent was removed under vacuum for less than 6 h. The dry lipid film was hydrated in 0.1 ml of 10 mM phosphate, 0.15 M NaCl, 0.1 mM EDTA (pH 7.4) by incubation for 3 h at 56°C. Samples were then pelleted in glass capillaries of 0.8 mm inner diameter, by using a bench-top centrifuge; excess supernatant was removed and the capillaries were flame sealed. Samples were incubated overnight at 4°C before measurement.

EPR measurements

EPR spectra were recorded at a microwave frequency of 9 GHz on a Bruker EMX EPR spectrometer (Bruker Biospin, Karlsruhe, Germany) equipped with nitrogen gas-flow temperature regulation. Sample capillaries were contained in a standard 4-mm quartz EPR sample tube that contained light silicone oil for thermal stability. Temperature was measured with a fine-wire thermocouple located within the EPR sample tube near the EPR sample capillary. The EPR sample tube was centered in the TE_{102} rectangular microwave cavity and all spectra were recorded under critical coupling conditions. The root-mean-square microwave magnetic field $\langle H_1^2\rangle^{1/2}$ at the sample was measured as described in reference (32). In-phase and out-of-phase EPR spectra were recorded in the first-harmonic absorption mode (V_1- and V_1'-displays, respectively) at modulation frequencies of 100 and 30 kHz. Out-of-phase V_1'-EPR spectra were recorded under conditions of microwave power saturation at $\langle H_1^2\rangle^{1/2} = 18$ μT, in phase-quadrature with the 100- or 30-kHz field modulation. Procedures for recording the nonlinear V_1'-EPR signals are described in references (29,30). The static magnetic field was measured with a Bruker ER 035M NMR magnetometer and the microwave frequency with a digital counter incorporated in the Bruker ER 041 XK-D bridge.

Data analysis

Experimental first-derivative EPR spectra from samples with different lipid compositions were normalized by dividing them by the second integral of the entire spectrum. The location of tie lines was explored by searching for isosbestic points in sets of normalized EPR spectra corresponding to different straight lines drawn in the coexistence regions of the ternary phase diagram. The appearance of isosbestic points, i.e., points where all spectra of the set intersect, indicates that these spectra represent two coexisting phases of constant composition, corresponding to the phase boundary endpoints, and differ only in the proportion of the two phases. It is important to note that there are unavoidable small differences in the microwave resonator frequency upon recording different samples and, therefore, the magnetic field scales of the EPR spectra were corrected to allow for these differences.

When a tie line is found, the compositions of the endpoints (i.e., phase boundaries) can be calculated from the compositions of samples lying on the tie line, together with the proportions of coexisting L_α and L_o phases in each sample, which are obtained from quantitative spectral subtraction (33). This is done by applying the lever rule (17,34,9). Allowance must

be made for the partition coefficient, K_p, of the spin-labeled phospholipid between the different phases. Details of the method are given in Section S.1 of the Supporting Material.

Coexisting phases are expected to be characterized by populations of spin-labeled lipids with different intrinsic spin-lattice relaxation times ($T_{1,e}$) (35), or with different relaxation enhancements induced by paramagnetic relaxants such as oxygen (36) or Ni perchlorate (37,30). Therefore, in addition to normal linear V_1-EPR spectra, nonlinear out-of-phase V_1'-EPR spectra (29) were also studied in the putative coexistence regions. Because the V_1'-EPR intensities of both spectral components depend directly on $T_{1,e}$ (29), in regions of phase coexistence, one expects a change in overall V_1'-EPR lineshape, relative to that of the conventional in-phase low-power V_1-EPR spectrum (30).

RESULTS

Ternary phase diagram of POPC/ PSM/chol membranes

Our strategy in determining phase boundaries was first to study the changes in EPR lineshapes and spectral parameters for binary lipid mixtures corresponding to a particular side of the Gibbs triangle (viz., 0 mol % PSM, 0 mol % POPC, or 0 mol % chol). Then spectral changes were investigated in a series of mixtures with fixed (nonzero) fractions of each of these components. Spin-labeled phosphatidylcholine with the nitroxide group situated towards the terminal methyl end of the sn-2 chain (14-PCSL or 16-PCSL) was used because this gives the best spectral resolution of coexisting lipid phases (17).

Left side of the Gibbs triangle: POPC/chol and low-PSM region

Conventional V_1-EPR spectra of the 14-PCSL spin label in binary POPC/chol mixtures (0 mol % PSM) are shown in the upper part of Fig. 1, for different compositions. The spectral anisotropy, $2\langle \Delta A \rangle = 2(\langle A_{max} \rangle - \langle A_{min} \rangle)$, increases gradually with increasing cholesterol content. At low cholesterol contents (≤ 10 mol %), the EPR lineshape of 14-PCSL has low hyperfine anisotropy ($2\langle \Delta A \rangle \approx 1.2 - 1.3$ mT) that is characteristic of the L_α state, and at high cholesterol contents (>30 mol %), it has a relatively large hyperfine anisotropy ($2\langle \Delta A \rangle \geq 2.2$ mT) characteristic of the L_o state.

The dependences of the hyperfine anisotropy, $2\langle \Delta A \rangle$, and outer hyperfine splitting, $2\langle A_{max} \rangle$, of 14-PCSL on cholesterol content in POPC/chol mixtures are given in the lower part of Fig. 1. No sharp transition in hyperfine anisotropy is seen over the range 0−60 mol % chol. Similar smooth dependences are observed for the EPR linewidths and amplitudes, which suggests that there are no phase boundaries along this composition line. If there were phase coexistence in this binary system, one should observe two-component spectra with isosbestic points. However, we detected neither two-component spectra nor any isosbestic points among the spectra for different compositions without PSM. This means that, over the range 0−60 mol % chol, phase separation does not occur along the 0 mol % PSM line at 23°C.
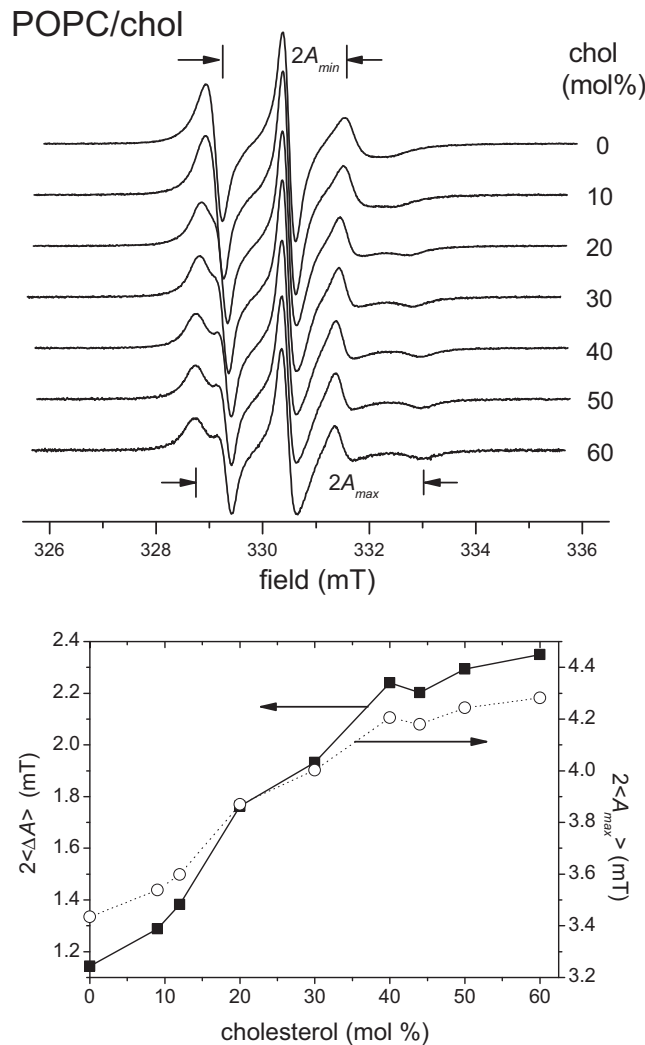
FIGURE 1 Top: Conventional V_1-EPR spectra of the 14-PCSL spin label in POPC/chol binary mixtures (0 mol % PSM), for different cholesterol contents as indicated. Bottom: Dependence on cholesterol content of the hyperfine anisotropy, $2\langle \Delta A \rangle = 2(\langle A_{max} \rangle - \langle A_{min} \rangle)$ (*solid squares*), and outer hyperfine splitting, $2\langle A_{max} \rangle$ (*open circles*), for the 14-PCSL spin label in POPC/chol membranes. $T = 23°C$.

Similar dependences on cholesterol content, without sharp transitions in the EPR parameters or isosbestic points, are found also for ternary mixtures with low and constant PSM content (up to 24 mol %). For 0 mol % PSM, these results suggest that the transition from the L_α to the L_o phase occurs continuously in this region.

In contrast to the POPC/chol system, two-component EPR spectra and several tie lines, along which the compositions of two coexisting phases are constant and only the relative proportions of the phases change, are detected for the binary mixtures, POPC/PSM and PSM/chol, and for corresponding ternary mixtures in the vicinity of 0 mol % chol and 0 mol % POPC, respectively. As shown below, these regions are attributed to the coexistence of gel and fluid

phases, L_β and L_α in the case of POPC/ PSM, and L_β and L_o in the case of PSM/chol.

Bottom of the Gibbs triangle: POPC/PSM and low-chol region

Representative conventional first-derivative V_1-EPR spectra of the 14-PCSL spin label in different binary mixtures of POPC/PSM without cholesterol are shown in Fig. 2. For ≤40 mol % PSM, the EPR lineshapes have relatively low hyperfine anisotropy ($2\langle A_{max}\rangle \cong 3.2$ mT) and broaden only weakly with increasing PSM content. Therefore, we attribute lipid compositions in this region, in the absence of cholesterol, to the L_α-phase. In the region of high PSM contents (≥50 mol %), two spectral components that have quite different lineshapes are clearly resolved. The weakly immobilized spectral component (w) is almost identical to the spectra for low PSM contents, whereas the more strongly immobilized component (s) has a large outer hyperfine splitting ($2\langle A_{max}\rangle \cong 5.9$ mT), which is almost indistinguishable from that for PSM alone (see Fig. 2). These two spectral components are attributed respectively to the L_α phase enriched in POPC and to the L_β gel phase enriched in PSM. Moreover, as seen from comparison of the EPR lineshapes and hyperfine splittings, the gel phase consists almost entirely of PSM. This means that POPC almost does not mix with the gel phase of PSM, at 23°C in the absence of cholesterol. The POPC-PSM line in the phase coexistence region of the two-component system must be a tie line in the ternary phase diagram. This is seen in Fig. 2, where the EPR spectra for 0 mol % chol and different POPC/PSM compositions clearly display isosbestic points (I).
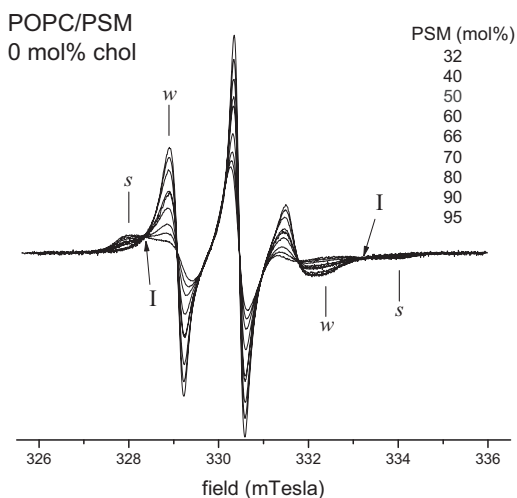

FIGURE 2 First-derivative V_1-EPR spectra of the 14-PCSL spin label in POPC/PSM binary mixtures (0 mol % chol). With decreasing line height, the spectra correspond to 32.5, 40, 50, 60, 66, 70, 80, 90, and 95.5 mol % PSM contents. Spectra are normalized to constant second integral. In the range 40−95.5 mol % PSM, the EPR spectra form an isosbestic set; I indicates isosbestic points. w and s indicate the outer hyperfine lines of the coexisting weakly and more strongly immobilized components, respectively. $T = 23$°C.

The dependence of the normalized intensity of the central EPR component (I_o) on PSM content shows a jump at ~40 mol % PSM that we take to be the left boundary of the $L_\alpha + L_\beta$ coexistence region. The right boundary, which is determined by disappearance of the w-component, is reached at very high contents of PSM ($\cong 95.5$ mol %, see Fig. 2). For even higher PSM contents, only the s-component is observed, corresponding to the single L_β-phase.

The EPR spectra in the $L_\alpha + L_\beta$ coexistence region can be represented as the weighted sums of w- and s-spectral components that correspond to the respective phase boundaries. The fractions, α and $1-\alpha$, of these components are determined from direct spectral subtraction by using normalized spectra at the phase boundaries for the single components, $\widehat{S}_{L_\alpha}$ and $\widehat{S}_{L_\beta}$. From the appropriate version of Eq. S8 in the Supporting Material, the average partition coefficient of 14-PCSL between L_α and L_β phases is then found to be $K_p(L_\alpha{:}L_\beta) = 1.06 \pm 0.1$.

The dependence of the 14-PCSL EPR lineshapes on PSM content in POPC/PSM mixtures that contain 3 mol % chol is similar to that for binary POPC/PSM mixtures lacking cholesterol. A tie line is identified at 3 mol % chol, over the range 40−77 mol % PSM. For samples containing 10 mol % chol, the situation is qualitatively similar to that at lower cholesterol content, except that the region of $L_\alpha - L_\beta$ phase coexistence is reduced in extent. A tie line over the range 40−70 mol % PSM is found for the samples with 10 mol % chol. These data at 3 and 10 mol % chol are described in Section S.2 of the Supporting Material.

Right side of the Gibbs triangle: PSM/chol and low-POPC region

First-derivative V_1-EPR spectra of the 14-PCSL spin label in different PSM/chol binary mixtures not containing POPC are shown in the upper panel of Fig. 3. For ≥40 mol % chol, only the w-component is present in the spectrum. However, the hyperfine anisotropy is appreciably greater than that for the L_α-phase. For a lipid mixture containing 60 mol % PSM and 40 mol % chol, the hyperfine anisotropy is $2\langle \Delta A\rangle = 2.71$ mT, as compared with $2\langle \Delta A\rangle \approx 0.9$ mT for the L_α-phase at the lower left side of the Gibbs triangle (see Fig. 1). Therefore, PSM/chol mixtures with ≥40 mol % chol are in the L_o-phase at 23°C.

At ≤10 mol % chol, only the s-component ($2\langle A_{max}\rangle \approx 5.9$ mT) is present in the EPR spectra, which indicates that PSM/chol mixtures are in a single L_β-phase at 23°C, for this composition range. For 10−30 mol % chol, overlapping s- and w-components are observed, indicating $L_o + L_\beta$ phase coexistence for these compositions. The lower panel of Fig. 3 gives the dependence of the normalized central amplitude on cholesterol content for the EPR spectra of PSM/chol mixtures. This exhibits an abrupt change at 38 mol % chol that corresponds to the boundary between the $L_o + L_\beta$ coexistence and L_o-phase regions. (The decreases at 0–6 and 50–60 mol % represent
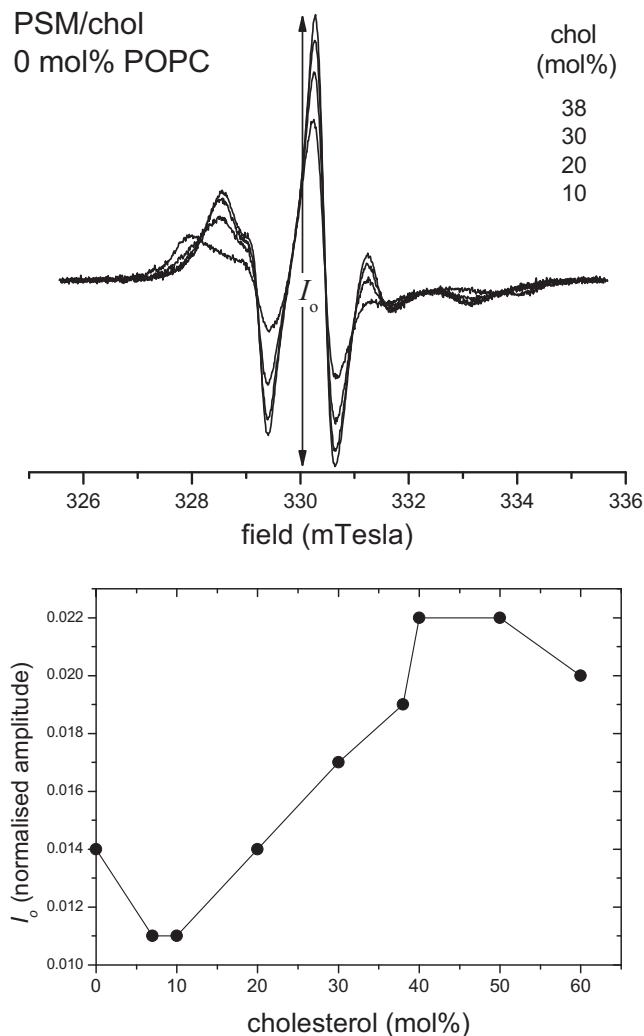
FIGURE 3 Top: First-derivative V_1-EPR spectra of the 14-PCSL spin label in PSM/chol binary mixtures (0 mol % POPC). With decreasing line height, the spectra correspond to 38, 30, 20, and 10 mol % cholesterol contents. Spectra are normalized to a constant second integral. In the range 10−38 mol % chol, the EPR spectra form an isosbestic set. Bottom: Dependence of the normalized line height, I_o, of the central peak in the 14-PCSL EPR spectrum (see *top panel*) on cholesterol content for PSM/chol membranes. $T = 23°C$.

gradual changes within single phases.) Close to the 38-mol % boundary, the s-component is not easily observed because of its greater width compared with that of the w-component. The set of EPR spectra for compositions in the range 15−38 mol % chol displays isosbestic points, as expected for two coexisting phases (see Fig. 3, *top*). An EPR signal from the L_o-phase is not seen for 10 mol % chol, although this composition fits well with the isosbestic set (see Fig. 3, *top*). Therefore, 10 mol % chol corresponds to the boundary between the L_β-phase and L_o+L_β coexistence region. Single-component EPR spectra corresponding to the L_o-phase are found for cholesterol contents >38 mol %. The average partition coefficient of 14-PCSL

between L_o- and L_β-phases in the coexistence region of PSM/chol mixtures is $K_p(L_o:L_\beta) = 2.5 \pm 0.2$, i.e., appreciably greater than unity.

Isosbestic points and tie lines are also found for sets of PSM/chol mixtures with constant POPC content of 4.5, 7, or 16.1 mol %. These data are described in Section S.3 of the Supporting Material.

The left (low PSM), bottom (low chol), and right (low POPC) sides of the phase diagram that are obtained on the basis of the above results with the 14-PCSL spin label are shown in Fig. 4. The entire ternary phase diagram is introduced already at this point because it facilitates subsequent presentation and discussion of further data. The heavy lines in the low-chol and low-POPC regions are tie lines for the $L_\alpha+L_\beta$ and L_o+L_β coexistence regions, respectively. Phase boundaries of the $L_\alpha+L_\beta$ and L_o+L_β coexistence regions are represented by nonheavy lines.

Central part of the Gibbs triangle

Conventional V_1-EPR spectra of the 16-PCSL spin label for POPC/PSM/chol mixtures in the central part of the Gibbs triangle (i.e., $0.65 > X_{POPC} > 0.1$, $0.25 < X_{PSM} < 0.65$, and $0.05 < X_{chol} < 0.30−0.35$) contain two spectral components from fluid lipid populations. This is indicative of $L_\alpha+L_o$ phase coexistence. Fig. 5 shows two isosbestic sets of 16-PCSL EPR spectra that correspond to tie lines in this region of the phase diagram at 23°C. The method of determining the tie-line endpoints is described in Section S.4 of the Supporting Material. The positions of the two tie lines corresponding to the isosbestic sets of spectra in
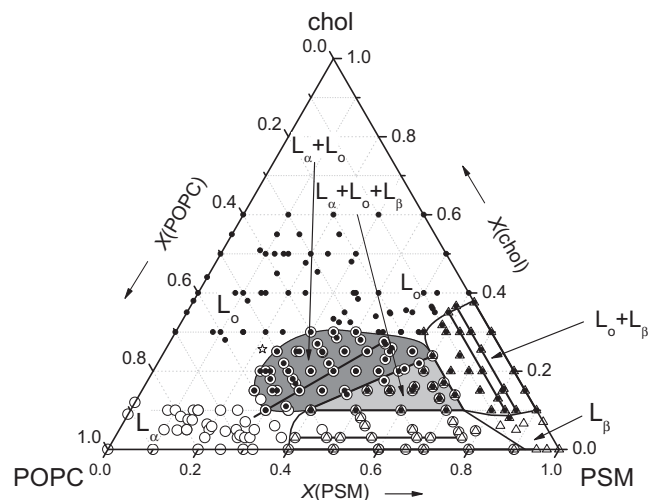

FIGURE 4 Ternary phase diagram for hydrated POPC/PSM/chol mixtures at 23°C constructed from the EPR results of this study. Symbols: ○, ●, △, ⊙, ◒, ▲, and ◉ refer to L_α, L_o, L_β, $L_\alpha+L_o$, $L_\alpha+L_\beta$, L_o+L_β, and $L_\alpha+L_o+L_\beta$ phases, respectively. The star indicates the approximate location of a putative critical point. Heavy straight lines within the $L_\alpha+L_\beta$, L_o+L_β, and $L_\alpha+L_o$ coexistence regions are tie lines. The three sides of the three-phase triangle are simultaneously tie lines in the neighboring two-phase regions.
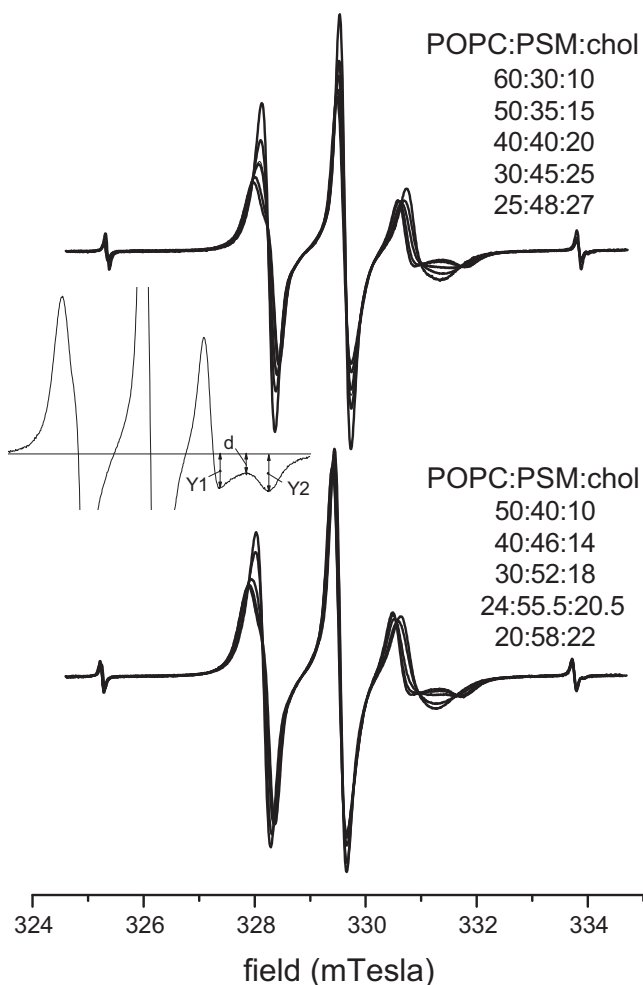
FIGURE 5 Isosbestic sets of first-derivative V_1-EPR spectra from the 16-PCSL spin label in POPC/PSM/chol membranes corresponding to tie lines in the central (*top panel*) and low (*bottom panel*) parts of the $L_\alpha+L_o$ coexistence region. With decreasing line height, the spectra correspond to the following POPC/PSM/chol compositions: 60:30:10, 50:35:15, 40:40:20, 30:45:25, and 25:48:27 mol/mol/mol (*top*); and 50:40:10, 40:46:14, 30:52:18, 24:55.5:20.5, and 20:58:22 mol/mol/mol (*bottom*). Spectra are normalized to constant second integral. $T = 23°C$. The fine-line spectrum in the top panel is obtained by weighted addition of spectra for POPC/PSM/chol compositions 60:30:10 and 30:45:25 mol/mol/mol, in the ratio 1:0.47. It is almost indistinguishable from the spectrum for POPC/PSM/chol composition 40:40:20 mol/mol/mol. The inset defines the parameters used in the subtraction procedure to establish the endpoint spectra; see text for details.

Fig. 5 are given by heavy straight lines in the phase diagram of Fig. 4. As shown immediately below, the tie line defined by the lower spectral set in Fig. 5 also constitutes the boundary with the three-phase triangle.

Three-phase region

Careful inspection of certain EPR lineshapes from the 14-PCSL and 16-PCSL spin labels in POPC/PSM/chol membranes, which have lower cholesterol content than that in the $L_\alpha+L_o$ phase coexistence region, reveals the presence of three spectral components. A strong immobilized *s*-component with outer hyperfine splitting $2\langle A_{max}\rangle \approx 5.9-6.0$ mT, which is attributed to the L_β phase, is present additionally to the two components in the rapid motion regime, which arise from the L_α and L_o phases. The L_β-component is identified in the low-field region as a shoulder or a broadening on the low-field side of the spectrum. In the high-field region, the L_β-component appears as an increased amplitude at the field position corresponding to the outer hyperfine line that specifies $2\langle A_{max}\rangle$. Usually, the L_α- and L_o-components are not fully resolved but can be identified by the intermediate lineshapes in the low- and high-field regions that arise from overlap of varying fractions of these two fluid components.

The existence of a three-phase triangle ($L_\alpha+L_o+L_\beta$) that adjoins the three two-phase coexistence regions ($L_\alpha+L_\beta$, $L_\alpha+L_o$, and L_o+L_β) is mandatory on thermodynamic grounds (see, e.g., 8). Our EPR spectral data allow assignment of putative boundaries for this triangle, which is depicted in light gray in Fig. 4. The base of the three-phase triangle is almost parallel to the base of the Gibbs triangle at ~10 mol % chol, and simultaneously is the boundary (and tie line) with the $L_\alpha+L_\beta$ two-phase coexistence region. The right side of the triangle at ~16 mol % POPC is the boundary (and tie line) with the L_o+L_β coexistence region, and the left side of the triangle is the boundary (and tie line) with the $L_\alpha+L_o$ coexistence region.

Thus, the complete phase diagram of the POPC/PSM/chol ternary system deduced from our EPR spectral analysis of 14-PCSL and 16-PCSL spin-labeled membranes is as presented in Fig. 4. It has one fluid-fluid ($L_\alpha+L_o$) and two gel-fluid ($L_\alpha+L_\beta$, L_o+L_β) two-phase coexistence regions, a three-phase ($L_\alpha+L_o+L_\beta$) coexistence region, and also regions corresponding to the single phases L_α, L_o, and L_β. Note that the phase boundaries in Fig. 4 slightly underestimate the size of the phase coexistence regions; because they are drawn through points that still contain a detectable amount of the second phase.

Nonlinear EPR evidence for phase coexistence

In the presence of lipid-soluble paramagnetic relaxation enhancement agents, lineshapes of the out-of-phase first-harmonic EPR spectra (V_1') were found to differ considerably from the conventional in-phase EPR spectra (V_1), for membranes within regions of phase coexistence. The reason is that the coexisting spectra components differ in their spin-lattice relaxation time. Spectra for two compositions in the $L_\alpha+L_o$ region, and one composition in the L_o+L_β coexistence region, are given in Fig. S3 of the Supporting Material. The nonlinear EPR spectra provide evidence, additional to that of two-component conventional EPR spectra and isosbestic points, for phase coexistence, and further substantiate the assignment of the $L_\alpha+L_o$ and L_o+L_β regions depicted in the ternary phase diagram of Fig. 4.

Spectral simulations for lipid dynamics in POPC/PSM/chol membranes

To estimate separately the orientational ordering and rotational diffusion of the lipid spin labels in different parts of the phase diagram, spectral simulations were performed by using a model of anisotropic molecular rotation in an orienting potential (38–40). These molecular dynamic parameters are particularly important in distinguishing the liquid-ordered and liquid-disordered phases (19). Results of spectral simulations are given in Section S.6 of the Supporting Material. For membranes with low (or zero) PSM content, the lipid chain order increases gradually with increasing cholesterol content, in a continuous transition from the L_α-phase (S_{zz}~0.1 for 14-PCSL at low cholesterol) to the L_o-phase (S_{zz}~0.4 for 14-PCSL at high cholesterol), with a small increase in rotational diffusion rate. In contrast, an abrupt change in order with increasing cholesterol content, via a region of L_α−L_o coexistence, is observed for membranes with constant intermediate POPC content (see Fig. S4 of the Supporting Material).

DISCUSSION

The regions of phase coexistence in the ternary lipid system PSM/POPC/chol are established here by using a spectral method that does not depend on the size of the domains, even when these are both fluid (as in L_α−L_o coexistence). Fig. 6 compares the present results with the phase diagrams obtained previously for the same system. For ease of comparison, the ternary phase diagrams are displayed as simple x-y plots, as described in reference (8). Note that the results with fluorescence microscopy (Fig. 6 middle) were published before the report recognizing the photochemical artifacts that could promote formation of large domains (24).

Our present phase diagram from spin-label EPR (Fig. 6, top) resembles more closely that of reference (11) from fluorescence microscopy of giant vesicles (Fig. 6, middle) than the original phase diagram of reference (25) that was deduced from the spectroscopic properties of fluorescent probes (Fig. 6, bottom). In particular, we do not find evidence for fluid-fluid phase separation for binary mixtures of POPC and cholesterol (left-hand y-axis of Fig. 6). Instead, we suggest a continuous transition between L_α and L_o phases in this region of the phase diagram, as described in detail in the Results section. Fluid-fluid phase separation in POPC/chol mixtures might not have been detected in reference (11), because the domains may be too small for light microscopy. This size limitation does not apply, however, to spin-label EPR studies. Indeed, L_α−L_o phase coexistence has been detected by spin-label EPR in binary mixtures of PSM and cholesterol (17), where none is seen by fluorescence microscopy.

Phase separation in the fluid regime of POPC/chol binary mixtures is also not detected by ^{2}H-NMR, whereas L_β−L_o
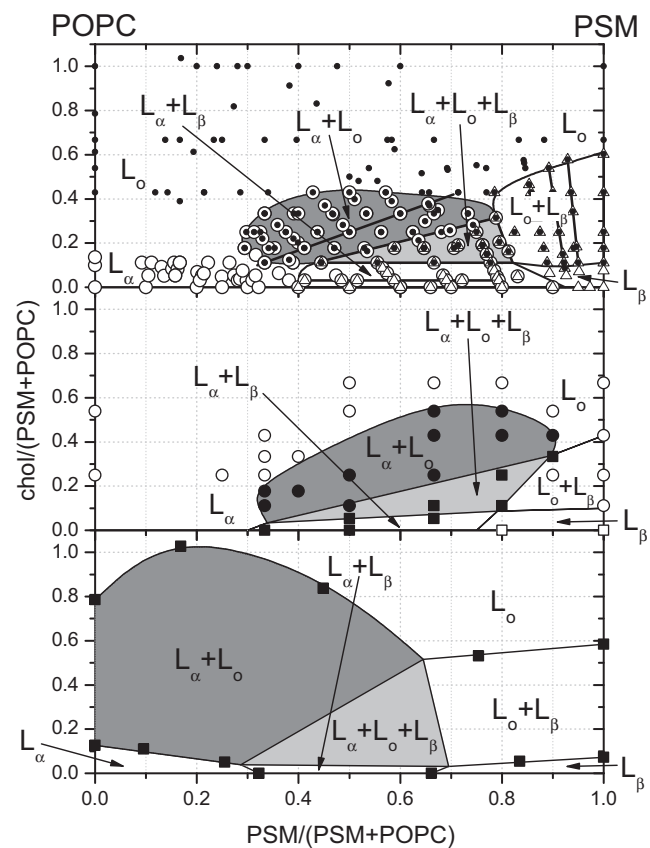

FIGURE 6 Ternary phase diagrams of hydrated POPC/PSM/chol mixtures at 23°C. Top: from spin-label EPR; this study (see Fig. 4). Middle: From fluorescence microscopy of giant vesicles (11). Open circles, single fluid phase; solid circles, coexisting fluid phases; open squares, absence of fluid phase; solid squares, presence of gel and fluid phases. Bottom: from fluorescence polarization of diphenylhexatriene and fluorescence lifetimes of *trans*-parinaric acid (25). Solid squares represent suggested phase boundaries. Phase diagrams are presented as described in reference (8).

phase coexistence is demonstrated by two-component spectra at lower temperatures (41). However, for fluorescence microscopy, this again might have been because the fluid domains are too small. Determinations of translational diffusion by pulsed field gradient NMR reveal no discontinuities in the dependence on cholesterol content for POPC/chol binary mixtures at 21°C, whereas discontinuities indicative of L_α−L_o phase coexistence are found in the fluid regime of SM/chol mixtures (42). This indicates the formation of a homogeneous phase in POPC/chol mixtures at 21°C and above, in agreement with the present spin-label EPR results. It was also concluded from δ-lysin induced dye efflux that POPC/chol mixtures do not exhibit phase separation over the temperature range 22−46°C (27). Possible reasons why indirect determinations of phase boundaries by fluorescent probes could be misleading are discussed in reference (6), although the appropriate conditions were fulfilled in reference (25). Interestingly, fluid-fluid phase separation is observed as two-component ^{2}H-NMR spectra in binary mixtures of POPC with ergosterol, although

this is said not to involve a L_o-phase (43) and such two-component spectra are not observed with POPC/chol mixtures (9).

Reasonably good agreement as to the position of the fluid-fluid (L_α–L_o) phase coexistence regime and of the three-phase triangle is found between the top and middle panels of Fig. 6. The agreement is less good, however, for the phase boundaries that involve the gel phase (L_β). In this connection, it should be noted that the L_β–L_o phase boundaries in reference (11) (Fig. 6, *middle*) were not identified by fluorescence microscopy but simply inferred. As regards the right-hand L_β–L_α phase boundary, differences from the spin-label EPR results could arise because of small domain sizes. It also should be remembered that translational diffusion in gel phases is very slow and therefore equilibrium might not be achieved readily, and the rate may depend on sample preparation.

Tie lines

Tie lines are of central importance because they map the trajectory of lipid compositions along which two coexisting phases (e.g., L_α and L_o) are identical and differ only in their relative proportions (44). Tie lines are straight for ternary diagrams depicted either as in Fig. 4 or as in Fig. 6 (8). The ends of the tie lines define the boundaries of phase coexistence, and simultaneously the compositions of the coexisting phases. Fig. 4 shows tie lines determined in each of the coexistence regions: L_α–L_β, L_β–L_o, and L_α–L_o. Note that within the three-phase triangle, the compositions of the coexisting phases are constant, specified by the three vertices.

Tie lines are also relevant to the question of how large a domain must be to constitute a thermodynamic phase. In the present context, the answer is that coexisting domains must obey the phase rule, in other words, ternary mixtures on a tie line must conform to the lever rule (Eq. S7). The existence of tie lines therefore confirms that Fig. 4 reflects phase equilibria, and not mesoscopic behavior in which the properties of the domain boundaries dominate over those of the domain interior.

Tie lines have not been determined previously for the POPC/PSM/chol sphingolipid-containing system, although some educated guesses were made in reference (25). This lack is hardly surprising because locating tie lines is not a particularly straightforward task for ternary systems; the present study involved investigation of >200 distinct compositions. However, tie lines have been determined by ^{2}H-NMR for two ternary systems in which a high chain-melting phosphatidylcholine acts as surrogate for the sphingolipid component (14–16). Recently, this has been augmented for L_α–L_o coexistence by an innovative approach with x-ray diffraction (45). The orientations of the tie lines that are found in these studies are similar to those for the sphingolipid-containing system in Fig. 4. For

L_α–L_β and L_β–L_o coexistence, the tie lines are roughly parallel to those for the corresponding binary mixtures, e.g., are inclined at a small angle to the X_{PSM} and X_{chol} axes, respectively, in Fig. 4. For fluid-fluid coexistence, the tie lines are roughly parallel to the diagonal in the phase diagram that specifies equimolar mixtures of PSM and cholesterol. The L_α–L_o tie line for POPC/PSM/chol in Fig. 6 is at 40° to the x axis (i.e., close to 45°), and in Fig. 4 is at ~0° to the perpendicular from the POPC vertex. From indirect determinations of L_o-phase populations in POPC/porcine brain SM/chol mixtures, it also was concluded that tie lines in the L_α–L_o coexistence region are roughly parallel to the equimolar SM/chol diagonal (27).

Not surprisingly, because of the difference in the proposed phase diagrams, the L_α–L_o tie lines determined in Fig. 4 differ considerably from the suggestion made for POPC/PSM/chol in reference (25). For the latter, the orientation of the L_α–L_o phase boundary of the three-phase triangle is 53° in the bottom panel of Fig. 6, as opposed to 30° for the present work in the top panel. Tie lines in the L_α–L_o coexistence region of dioleoyl PC/brain SM/chol ternary mixtures were presented in reference (28). These are derived from spin-label EPR measurements, but experimental details are not given. The L_α–L_o tie lines illustrated in this reference are inclined at a greater angle (−14° to −23°) to the equimolar PSM/chol diagonal than that for POPC/PSM/chol (0° to +7°) in Fig. 4. In fact, they depart even further in orientation from the direct determinations in Fig. 4 and references (14–16) than do the indirect predictions in reference (25).

Miscibility critical points

Tie-line orientations in the L_α–L_o coexistence region in Fig. 4 tilt away from the horizontal on going from the three-phase boundary into the two-phase region. A critical point occurs at the point at which the length of the tie line finally reduces to zero and merges with the outer phase boundary. The approximate point at which this is predicted to occur is indicated by the star in Fig. 4. It is located adjacent to the region of continuous transition from the L_α phase (*open circles*) to the L_o phase (*solid dots*) that is characterized by intermediate values of the hyperfine anisotropy, $2\langle\Delta A\rangle$ (cf. Fig. 1). As the critical point is approached, the difference between the L_α and L_o phases decreases making them more difficult to distinguish in the EPR spectrum. Therefore, it is likely the true critical point resides in a region that is designated as single-phase in Fig. 4, as is indicated.

Note that the orientation of the putative tie line through the point (1,1,1) that was proposed in reference (25) is consistent with the position of the critical point shown in Fig. 4. Regions of approximately constant energy transfer efficiency at the ends of this putative tie line (22) could suggest that it should be shorter, which is also consistent with the phase boundaries in Fig. 4.

Critical points are of interest because they correspond to states with large fluctuations in lipid packing/ordering and in local composition. These critical fluctuations are observed in the domains visualized by fluorescence microscopy ([16]), and are manifest as T_2-relaxation enhancements and line broadening in ^{2}H-NMR ([14]). To the extent that it might be found in biological membranes containing cholesterol, the fluctuating state could have important functional consequences.

CONCLUSION

This work largely resolves the disagreement in the literature regarding $L_\alpha-L_o$ phase coexistence in POPC/PSM/chol ternary systems (for a review, see ([9])). Using a method that is not dependent on domain size, it is found here that the failure to detect fluid-fluid phase separation at low (or zero) PSM contents is not because the domains are too small to be detected by fluorescence microscopy. Simply, conversion between L_α and L_o phases takes place via a continuous transition in this region of the phase diagram, although one knowledgeable reviewer still dissents from this interpretation, and there remains the different behavior of ergosterol ([43]).

As pointed out already ([25]), the POPC/PSM/chol system represents the simplest fully defined model membrane that incorporates all lipid components thought to be essential for raft formation in natural membranes. In so far as the existence of lipid rafts can be identified with coexistence of L_α and L_o phases, the tie lines that are determined here establish the lipid compositions, and hence properties, which such lipid rafts can assume.

SUPPORTING MATERIAL

REFERENCES

1. Simons, K., and E. Ikonen. 1997. Functional rafts in cell membranes. *Nature.* 387:569–572.

2. Simons, K., and W. L. Vaz. 2004. Model systems, lipid rafts, and cell membranes. *Annu. Rev. Biophys. Biomol. Struct.* 33:269–295.

3. Lingwood, D., and K. Simons. 2010. Lipid rafts as a membrane-organizing principle. *Science.* 327:46–50.

4. Vist, M. R., and J. H. Davis. 1990. Phase equilibria of cholesterol/dipalmitoylphosphatidylcholine mixtures: ^{2}H nuclear magnetic resonance and differential scanning calorimetry. *Biochemistry.* 29:451–464.

5. Ipsen, J. H., G. Karlström, …, M. J. Zuckermann. 1987. Phase equilibria in the phosphatidylcholine-cholesterol system. *Biochim. Biophys. Acta.* 905:162–172.

6. Marsh, D. 2010. Liquid-ordered phases induced by cholesterol: a compendium of binary phase diagrams. *Biochim. Biophys. Acta.* 1798:688–699.

7. Recktenwald, D. J., and H. M. McConnell. 1981. Phase equilibria in binary mixtures of phosphatidylcholine and cholesterol. *Biochemistry.* 20:4505–4510.

8. Marsh, D. 2009. Cholesterol-induced fluid membrane domains: a compendium of lipid-raft ternary phase diagrams. *Biochim. Biophys. Acta.* 1788:2114–2123.

9. Goñi, F. M., A. Alonso, …, J. L. Thewalt. 2008. Phase diagrams of lipid mixtures relevant to the study of membrane rafts. *Biochim. Biophys. Acta.* 1781:665–684.

10. Veatch, S. L., and S. L. Keller. 2003. Separation of liquid phases in giant vesicles of ternary mixtures of phospholipids and cholesterol. *Biophys. J.* 85:3074–3083.

11. Veatch, S. L., and S. L. Keller. 2005. Miscibility phase diagrams of giant vesicles containing sphingomyelin. *Phys. Rev. Lett.* 94:148101.

12. Zhao, J., J. Wu, …, G. Feigenson. 2007. Phase studies of model biomembranes: macroscopic coexistence of $L_\alpha+L_\beta$, with light-induced coexistence of $L_\alpha+L_o$ Phases. *Biochim. Biophys. Acta.* 1768:2777–2786.

13. Zhao, J., J. Wu, …, G. W. Feigenson. 2007. Phase studies of model biomembranes: complex behavior of DSPC/DOPC/cholesterol. *Biochim. Biophys. Acta.* 1768:2764–2776.

14. Veatch, S. L., O. Soubias, …, K. Gawrisch. 2007. Critical fluctuations in domain-forming lipid mixtures. *Proc. Natl. Acad. Sci. USA.* 104:17650–17655.

15. Davis, J. H., J. J. Clair, and J. Juhasz. 2009. Phase equilibria in DOPC/DPPC-d$_{62}$/cholesterol mixtures. *Biophys. J.* 96:521–539.

16. Veatch, S. L., K. Gawrisch, and S. L. Keller. 2006. Closed-loop miscibility gap and quantitative tie-lines in ternary membranes containing diphytanoyl PC. *Biophys. J.* 90:4428–4436.

17. Collado, M. I., F. M. Goñi, …, D. Marsh. 2005. Domain formation in sphingomyelin/cholesterol mixed membranes studied by spin-label electron spin resonance spectroscopy. *Biochemistry.* 44:4911–4918.

18. Veiga, M. P., J. L. R. Arrondo, …, D. Marsh. 2001. Interaction of cholesterol with sphingomyelin in mixed membranes containing phosphatidylcholine, studied by spin-label ESR and IR spectroscopies. A possible stabilization of gel-phase sphingolipid domains by cholesterol. *Biochemistry.* 40:2614–2622.

19. Chiang, Y. W., Y. Shimoyama, …, J. H. Freed. 2004. Dynamic molecular structure of DPPC-DLPC-cholesterol ternary lipid system by spin-label electron spin resonance. *Biophys. J.* 87:2483–2496.

20. Chiang, Y. W., J. Zhao, …, G. W. Feigenson. 2005. New method for determining tie-lines in coexisting membrane phases using spin-label ESR. *Biochim. Biophys. Acta.* 1668:99–105.

21. Heberle, F. A., J. Wu, …, G. W. Feigenson. 2010. Comparison of three ternary lipid bilayer mixtures: FRET and ESR reveal nanodomains. *Biophys. J.* 99:3309–3318.

22. de Almeida, R. F. M., L. M. S. Loura, …, M. Prieto. 2005. Lipid rafts have different sizes depending on membrane composition: a time-resolved fluorescence resonance energy transfer study. *J. Mol. Biol.* 346:1109–1120.

23. Pathak, P., and E. London. 2011. Measurement of lipid nanodomain (raft) formation and size in sphingomyelin/POPC/cholesterol vesicles shows TX-100 and transmembrane helices increase domain size by coalescing preexisting nanodomains but do not induce domain formation. *Biophys. J.* 101:2417–2425.

24. Ayuyan, A. G., and F. S. Cohen. 2006. Lipid peroxides promote large rafts: effects of excitation of probes in fluorescence microscopy and electrochemical reactions during vesicle formation. *Biophys. J.* 91:2172–2183.

25. de Almeida, R. F. M., A. Fedorov, and M. Prieto. 2003. Sphingomyelin/phosphatidylcholine/cholesterol phase diagram: boundaries and composition of lipid rafts. *Biophys. J.* 85:2406–2416.

26. Thompson, T. E., and T. W. Tillack. 1985. Organization of glycosphingolipids in bilayers and plasma membranes of mammalian cells. *Annu. Rev. Biophys. Biophys. Chem.* 14:361–386.

27. Pokorny, A., L. E. Yandek, …, P. F. Almeida. 2006. Temperature and composition dependence of the interaction of δ-lysin with ternary mixtures of sphingomyelin/cholesterol/POPC. *Biophys. J.* 91:2184–2197.

28. Smith, A. K., and J. H. Freed. 2009. Determination of tie-line fields for coexisting lipid phases: an ESR study. *J. Phys. Chem. B.* 113:3957–3971.

29. Livshits, V. A., T. Páli, and D. Marsh. 1998. Spin relaxation measurements using first-harmonic out-of-phase absorption EPR signals. *J. Magn. Reson.* 134:113–123.

30. Livshits, V. A., and D. Marsh. 2005. Application of the out-of-phase absorption mode to separating overlapping EPR signals with different T_1 values. *J. Magn. Reson.* 175:317–329.

31. Marsh, D. 2008. Electron spin resonance in membrane research: protein-lipid interactions. *Methods.* 46:83–96.

32. Fajer, P., and D. Marsh. 1982. Microwave and modulation field inhomogeneities and the effect of cavity Q in saturation transfer ESR spectra. Dependence on sample size. *J. Magn. Reson.* 49:212–224.

33. Knowles, P. F., A. Watts, and D. Marsh. 1981. Spin-label studies of head-group specificity in the interaction of phospholipids with yeast cytochrome oxidase. *Biochemistry.* 20:5888–5894.

34. Silvius, J. R. 2005. Partitioning of membrane molecules between raft and non-raft domains: insights from model-membrane studies. *Biochim. Biophys. Acta.* 1746:193–202.

35. Livshits, V. A., B. G. Dzikovski, and D. Marsh. 2003. Anisotropic motion effects in CW non-linear EPR spectra: relaxation enhancement of lipid spin labels. *J. Magn. Reson.* 162:429–442.

36. Subczynski, W. K., J. Widomska, …, A. Kusumi. 2007. Saturation recovery electron paramagnetic resonance discrimination by oxygen transport (DOT) method for characterizing membrane domains. *In* Lipid Rafts. T. J. McIntosh, editor. Humana Press, Totowa, New Jersey. 143–157.

37. Livshits, V. A., B. G. Dzikovski, and D. Marsh. 2001. Mechanism of relaxation enhancement of spin labels in membranes by paramagnetic ion salts: dependence on 3*d* and 4*f* ions and on the anions. *J. Magn. Reson.* 148:221–237.

38. Schneider, D. J., and J. H. Freed. 1989. Calculating slow motional magnetic resonance spectra: a user's guide. *In* Spin-Labeling. Theory and Applications. L. J. Berliner and J. Reuben, editors. Plenum Publishing, New York. 1–76.

39. Budil, D. E., S. Lee, …, J. H. Freed. 1996. Nonlinear least-squares analysis of slow-motion EPR spectra in one and two dimensions using a modified Levenberg-Marquardt algorithm. *J. Magn. Reson. A.* 120:155–189.

40. Livshits, V. A., D. Kurad, and D. Marsh. 2006. Multifrequency simulations of the EPR spectra of lipid spin labels in membranes. *J. Magn. Reson.* 180:63–71.

41. Thewalt, J. L., and M. Bloom. 1992. Phosphatidylcholine: cholesterol phase diagrams. *Biophys. J.* 63:1176–1181.

42. Filippov, A., G. Orädd, and G. Lindblom. 2003. The effect of cholesterol on the lateral diffusion of phospholipids in oriented bilayers. *Biophys. J.* 84:3079–3086.

43. Hsueh, Y. W., M. T. Chen, …, J. Thewalt. 2007. Ergosterol in POPC membranes: physical properties and comparison with structurally similar sterols. *Biophys. J.* 92:1606–1615.

44. Cevc, G., and D. Marsh. 1987. Phospholipid Bilayers: Physical Principles and Models. Wiley-Interscience, New York.

45. Uppamoochikkal, P., S. Tristram-Nagle, and J. F. Nagle. 2010. Orientation of tie-lines in the phase diagram of DOPC/DPPC/cholesterol model biomembranes. *Langmuir.* 26:17363–17368.